nature COMMUNICATIONS

ARTICLE

Received 26 Nov 2012 | Accepted 25 Feb 2013 | Published 3 April 2013

DOI: 10.1038/ncomms2659

Reconciliation of marine and terrestrial carbon isotope excursions based on changing atmospheric CO_2 levels

Brian A. Schubert[1,†] & A. Hope Jahren[1]

Negative carbon isotope excursions measured in marine and terrestrial substrates indicate large-scale changes in the global carbon cycle, yet terrestrial substrates characteristically record a larger-amplitude carbon isotope excursion than marine substrates for a single event. Here we reconcile this difference by accounting for the fundamental increase in carbon isotope fractionation by land plants in response to increasing atmospheric CO_2 concentration (pCO_2). We show that for any change in pCO_2 concentration (ΔpCO_2), terrestrial and marine records can be used together to reconstruct background and maximum pCO_2 levels across the carbon isotope excursion. When applied to the carbon isotope excursion at the Palaeocene–Eocene boundary, we calculate $pCO_2 = 674$–$1{,}034$ p.p.m.v. during the Late Palaeocene and 1,384–3,342 p.p.m.v. during the height of the carbon isotope excursion across all sources postulated for the carbon release. This analysis demonstrates the need to account for changing pCO_2 concentration when analysing large-scale changes in the carbon isotope composition of terrestrial substrates.

[1] University of Hawai'i at Mānoa, Department of Geology and Geophysics, Honolulu, Hawai'i 96822, USA. [†] Present address: School of Geosciences, University of Louisiana at Lafayette, 611 McKinley Street, Box 44530, Hamilton Hall #323, Lafayette, Louisiana 70504, USA. Correspondence and requests for materials should be addressed to B.A.S. (email: schubert@louisiana.edu).

Globally correlated, negative excursions in carbon isotope ($\delta^{13}C$) values measured in marine and terrestrial substrates throughout the Phanerozoic indicate episodic, massive additions of isotopically depleted carbon to the ocean–atmosphere system[1–10]. These events not only changed the carbon isotope composition of atmospheric carbon dioxide ($\delta^{13}C_{CO2}$), but also raised pCO_2 concentrations (for example, ref. 11). The magnitude of the carbon isotope excursion (CIE) and the amount of pCO_2 rise (ΔpCO_2) calculated for such events should relate to one another, and the source of the carbon input and changes in the global carbon cycle have been reconstructed upon this premise (for example, refs 5,9,11,12). Determination of the 'true' magnitude of a CIE (that is, the amount of the CIE caused only by the change in $\delta^{13}C_{CO2}$) is fundamental to calculating the amount of carbon added to the atmosphere at the event and improving our understanding of feedbacks in the climate system[13,14].

One complicating factor is that the magnitude of the CIE is characteristically larger when measured in terrestrial versus marine substrates by up to several per mil[6–9,11,15]. Workers have argued that larger-magnitude negative excursions recorded in terrestrial substrates reflect increased humidity or precipitation[6,7] based on the increased carbon isotope fractionation that modern land plants demonstrate in response to these environmental factors. Others have attributed this difference to an increased abundance of angiosperm flora, which are characteristically isotopically depleted in comparison with gymnosperm flora[16,17]. Both of these mechanisms are problematic as general explanations for any global discrepancy between terrestrial and marine CIEs because their influences are most likely to be locally and heterogeneously expressed[15,18] (Supplementary Information). Moreover, changes in angiosperm abundance cannot explain larger terrestrial versus marine CIEs in pre-Cretaceous substrates (for example, ref. 7). The reconciliation of terrestrial versus marine CIEs requires a mechanism fundamental to all C_3 photosynthesis, and thus globally applicable (we note that classical C_4 photosynthesis is a recent evolutionary innovation, relegated to no more than the last $\sim$13 million years of Earth's history[19,20], and that CAM photosynthesis is largely limited to aqueous and desert environments).

Previous experiments have shown that the carbon isotope value of plant tissues ($\delta^{13}C_p$) is affected by changes in pCO_2 concentration, independent of changes in $\delta^{13}C_{CO2}$, and identified a positive relationship between pCO_2 concentration and carbon isotope fractionation ($\Delta\delta^{13}C_p \approx \delta^{13}C_{CO2} - \delta^{13}C_p$) in both angiosperm and gymnosperm taxa (for example, refs 21,22; Supplementary Information). More recently, time-series correlations between climate variables and tree-ring $\Delta\delta^{13}C_p$ values have been shown to improve when a correction proportional to the increase in pCO_2 is applied (for example, refs 23–25). However, a wide range of corrections for the effect of changing pCO_2 on $\Delta\delta^{13}C_p$ (S; ‰/p.p.m.v.) have been reported and applied, typically ranging from $S = 0.73$ to 2.0‰ per 100 p.p.m.v. increase in pCO_2 (for example, refs 23,24; Supplementary Information).

Our recent work growing plants under controlled environmental conditions across a wide range of pCO_2 levels (up to 4,200 p.p.m.v.) provided a unifying relationship for the effect of pCO_2 on C_3 plant tissue, showing that S decreases systematically with increasing pCO_2 across a wide range of C_3 plants ($R = 0.96$, $n = 33$) (Fig. 1) (ref. 26). This relationship suggests that for any large release of isotopically depleted carbon to the ocean or atmosphere, the land-plant-derived substrates of the terrestrial record ($CIE_{terrestrial}$; that is, terrestrial organic matter, soil carbonate, plant lipids and tooth enamel) will record a larger-amplitude CIE than marine substrates (CIE_{marine}; that is, benthic foraminifera, planktic foraminifera and bulk marine carbonate). Thus, we propose that the difference in magnitude between these two substrates ($\Delta CIE = CIE_{terrestrial} - CIE_{marine}$) results from the additional fractionation by land plants due to rising pCO_2 levels, which is then propagated within the terrestrial record. We apply this to the particularly well-studied and globally widespread CIE at the Palaeocene–Eocene Thermal Maximum (PETM), for which analysis of >150 CIEs shows a significant, 2.1‰ greater amplitude CIE recorded in terrestrial versus marine substrates[11], in order to calculate absolute pCO_2 levels during the Late Palaeocene and at the height of the CIE for the range of sources (and thus, ΔpCO_2 values) postulated for the carbon release.

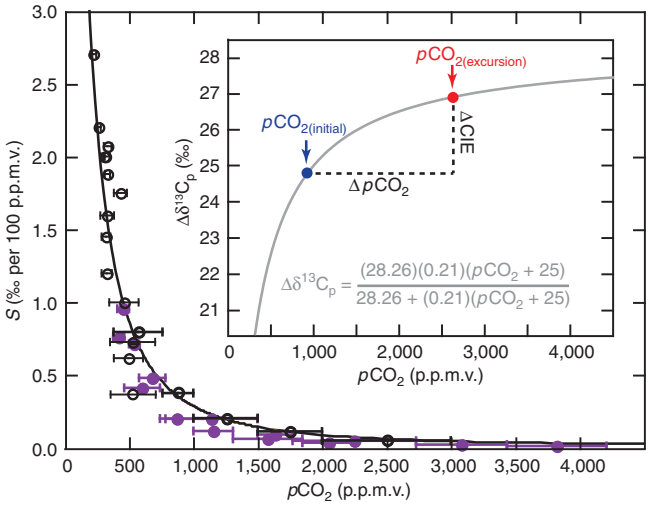

Figure 1 | The effect of pCO_2 concentration on C_3 land-plant carbon isotope fractionation. Across field and chamber experiments on a wide range of C_3 land-plant species, the amount of carbon-isotope fractionation per change in pCO_2 (S, ‰ per p.p.m.v.) decreases within increasing pCO_2 level according to the following equation: $S = (B)(A^2)/[A + B(pCO_2 + C)]^2$ with $R = 0.96$ ($n = 33$) (black curve), where $A = 28.26$, $B = 0.21$ and $C = 25$. Purple closed circles reflect data from our experiments[26]; open black circles represent data compiled from published studies (Supplementary Table S2). Horizontal bars encompass the range of pCO_2 levels used within each experiment; the circle is plotted at the midpoint of the range. The grey curve (inset) represents the integral of the black curve, and follows the general hyperbolic relationship: $\Delta\delta^{13}C_p = [(A)(B)(pCO_2 + C)]/[A + (B)(pCO_2 + C)]$ (see Supplementary Information). As the relationship between pCO_2 and $\Delta\delta^{13}C_p$ is nonlinear, absolute estimates of $pCO_{2(initial)}$ (blue) and $pCO_{2(excursion)}$ (red) can be calculated by solving equations (1) and (2) provided ΔpCO_2 and ΔCIE are known (dashed lines); for a given magnitude CIE, the ΔpCO_2 estimate is dependent on the $\delta^{13}C$ value of the source. Figure is modified from ref. 26 with new data reported in Lomax *et al.*[59] (Supplementary Information; Supplementary Table S1).

Results

Reconciliation of ΔCIE *via* the pCO_2 effect. The larger-magnitude CIE recorded in terrestrial versus marine substrates can be described by the following equation relating ΔCIE to the effect of changing pCO_2 levels on carbon isotope fractionation by C_3 land plants:

$$\Delta CIE = \frac{(A)(B)(pCO_{2(initial)} + C)}{A + (B)(pCO_{2(initial)} + C)} - \frac{(A)(B)(pCO_{2(excursion)} + C)}{A + (B)(pCO_{2(excursion)} + C)} \quad (1)$$

where $pCO_{2(initial)}$ and $pCO_{2(excursion)}$ are the pCO_2 levels immediately before and at the height of the CIE, respectively, and A, B and C are constants produced by the best-fit curve through the

experimental data and published values (Fig. 1 inset and Supplementary Information). For CIE events where the magnitude of both $CIE_{terrestrial}$ and CIE_{marine} are well-documented globally, knowledge of ΔCIE can be used towards the determination of both $pCO_{2(initial)}$ and $pCO_{2(excursion)}$ provided the change in pCO_2 (ΔpCO_2) is known (Fig. 1 inset):

$$\Delta pCO_2 = pCO_{2(excursion)} - pCO_{2(initial)} \quad (2)$$

Estimates of ΔpCO_2, which are dependent on the true magnitude of the CIE and the $\delta^{13}C$ value of the source ($\delta^{13}C_{source}$), are commonly calculated using methods ranging from mass balance equations (for example, refs 5,11) to numerical models (for example, refs 12,27). Therefore, provided independent estimates of ΔCIE and ΔpCO_2, equations (1) and (2) can be solved simultaneously for absolute estimates of $pCO_{2(initial)}$ and $pCO_{2(excursion)}$ (Fig. 2), allowing for a wholly new quantitative reconstruction of changes in the global carbon cycle. Although determination of $pCO_{2(initial)}$ and $pCO_{2(excursion)}$ requires precise estimates of ΔCIE and ΔpCO_2, Fig. 2 shows that the value for $pCO_{2(initial)}$ is more sensitive to ΔCIE than to ΔpCO_2, while $pCO_{2(excursion)}$ is more sensitive to ΔpCO_2 than to ΔCIE.

Determination of pCO_2 levels across the CIE at the PETM. The highly studied, globally widespread CIE that marks the PETM represents an ideal event upon which to first apply our methods to quantify $pCO_{2(initial)}$ and $pCO_{2(excursion)}$ because of the large number of $CIE_{terrestrial}$ and CIE_{marine} records that can be used to provide a robust estimate of ΔCIE globally. More than 150 total CIE_{marine} and $CIE_{terrestrial}$ records have been measured across the PETM (reviewed by McInerney and Wing[11]); the average CIE measured in terrestrial substrates that include soil carbonate, plant lipids, bulk soil organic matter and tooth enamel ($CIE_{terrestrial} \pm 1\sigma = -4.7 \pm 1.5$‰, $n = 48$) is 2.1‰ more negative than that measured in benthic foraminifera, planktic foraminifera and bulk marine carbonate from marine environments ($CIE_{marine} \pm 1\sigma = -2.6 \pm 1.1$‰, $n = 105$) (ΔCIE = −2.1‰). Bulk marine organic matter was not included in our determination of CIE_{marine} because it can include mixed pools of carbon from photosynthetic and non-photosynthetic organisms from terrestrial and marine environments[15,28–30]. By averaging across the large number of diverse sites and substrates available for the PETM, biasing effects of local and regional changes in climate[6,8,31–39], vegetation[16,17,38], sediment transport[40,41], salinity[15,42] and dissolution[43,44] on ΔCIE are limited. Using this ΔCIE value (−2.1‰), Late Palaeocene ($pCO_{2(initial)}$) and PETM ($pCO_{2(excursion)}$) pCO_2 levels can be determined across a range of ΔpCO_2 estimates by simultaneously solving equations (1) and (2) (Fig. 3).

Reconstructed estimates of $pCO_{2(initial)}$ and $pCO_{2(excursion)}$ increase as ΔpCO_2 increases (Fig. 3); thus the solution based on a methane hydrate source ($\delta^{13}C_{source} = -60$‰, $\Delta pCO_2 =$ 710 p.p.m.v.) yielded the lowest Late Palaeocene pCO_2 estimate ($pCO_{2(initial)} = 674$ p.p.m.v.), followed by thermogenic methane or permafrost thawing ($\delta^{13}C_{source} = -30$‰, $\Delta pCO_2 = 1{,}566$ p.p.m.v.) that yielded $pCO_{2(initial)} = 915$ p.p.m.v., and then wildfire or drying of epicontinental seas ($\delta^{13}C_{source} = -22$‰, $\Delta pCO_2 =$ 2,308 p.p.m.v.) having the highest Late Palaeocene pCO_2 estimate ($pCO_{2(initial)} = 1{,}034$ p.p.m.v.). If these sources can be thought to exhaust the carbon isotope range of potential sources, we calculate that Late Palaeocene pCO_2 levels may have been as low as ~280 p.p.m.v. higher than present, and were much lower than the recent pCO_2 estimates for the year 2300 (refs 45,46; Fig. 3). pCO_2 levels at the peak of the PETM were calculated to be 1,384, 2,481 and 3,342 p.p.m.v. for methane hydrate, thermogenic methane or permafrost thawing, and drying of epicontinental seas or wildfire sources ($\Delta pCO_2 = 710$, 1,566 and 2,308 p.p.m.v.), respectively (Fig. 3).

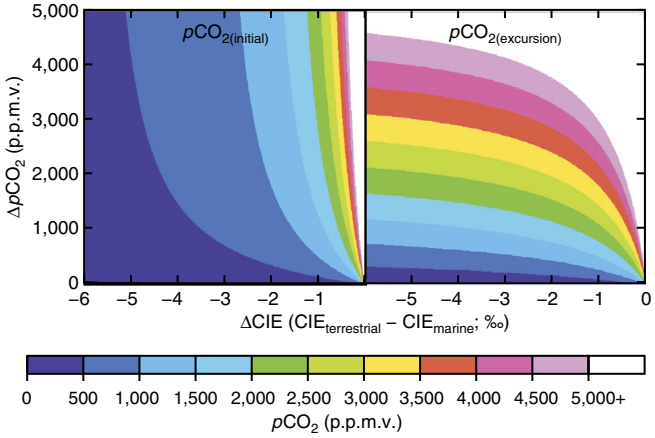

Figure 2 | Determination of pCO_2 levels as a function of ΔCIE and ΔpCO_2. For any hypothetical CIE, $pCO_{2(initial)}$ (left) and $pCO_{2(excursion)}$ (right) are a function of the difference between the terrestrial and marine CIE (ΔCIE; $\Delta CIE = CIE_{terrestrial} - CIE_{marine}$) and the rise in pCO_2 (ΔpCO_2; $\Delta pCO_2 = pCO_{2(excursion)} - pCO_{2(initial)}$). Values for $pCO_{2(initial)}$ and $pCO_{2(excursion)}$ were calculated by solving equations (1) and (2) simultaneously.

Discussion

Determination of Late Palaeocene and PETM pCO_2 levels is important for quantifying climate sensitivity to CO_2 for this greenhouse period (for example, ref. 47); however, previous proxy estimates for the Late Palaeocene are highly varied, ranging from 100 to 2,400 p.p.m.v., and robust PETM pCO_2 estimates are lacking (Supplementary Information; Fig. 3). Across a wide range of increases in pCO_2 at the PETM ($\Delta pCO_2 \leq 3{,}000$ p.p.m.v.), our results indicate that Late Palaeocene pCO_2 levels were ≤ 1,112 p.p.m.v. (Fig. 3). If we consider a relatively small increase in pCO_2 levels ($\Delta pCO_2 < 1{,}000$ p.p.m.v.), as would be attributed to a methane hydrate source, our Late Palaeocene pCO_2 estimates are consistent with values determined from liverwort, phytoplankton and stomatal proxies (Fig. 3). The boron isotope proxy, in contrast, is more consistent with our results assuming that the amount of pCO_2 increase was larger (> 1,000 p.p.m.v.), as would be required for the thawing permafrost model, for example (Fig. 3).

Although our reconciliation does not allow for the determination of the carbon source of the CIE at the PETM, recent work indicates significant warming before the onset of the CIE (refs 33,48), and suggests an orbitally forced mechanism for the release of carbon at the event[49–51]. If we consider the two hypotheses suggesting that orbital forcing triggered the release of carbon through a methane hydrate release (ref. 49) ($\Delta pCO_2 = 710$ p.p.m.v.) or large-scale thawing of permafrost (ref. 50) ($\Delta pCO_2 = 1{,}566$ p.p.m.v.), we calculate Late Palaeocene pCO_2 levels = 674 (+159 −109) or 915 (+225 −153) p.p.m.v., respectively (error based on ΔCIE = −1.6 to −2.6‰; Fig. 3). Notably, these calculated values for Late Palaeocene pCO_2 are consistent with the pCO_2 levels required by Lunt *et al.*[49] (~560 p.p.m.v.) and DeConto *et al.*[50] (~900 p.p.m.v.) for each of their respective models.

Many arguments have been made to explain the larger CIE measured in terrestrial versus marine substrates at the PETM[6,8,15–18,42,43], but each requires additional phenomena secondary to the carbon release (Supplementary Information).

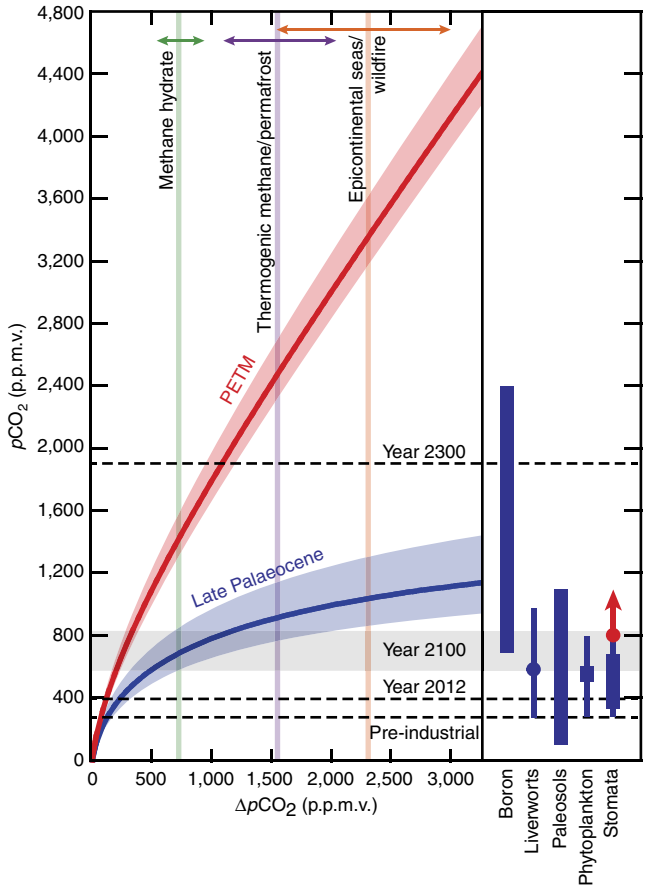

Figure 3 | Reconstruction of pCO_2 levels during the Late Palaeocene and PETM. Across a range of possible pCO_2 increases (ΔpCO_2), pCO_2 levels for the Late Palaeocene (blue curve; $pCO_{2(initial)}$) and PETM (red curve; $pCO_{2(excursion)}$) were calculated by simultaneously solving equations (1) and (2) for $\Delta pCO_2 = 0$–3,600 p.p.m.v. and $\Delta CIE = -2.1‰$ (thick curves). Blue and red shaded regions show solutions for $\Delta CIE = -1.6$ to $-2.6‰$ to illustrate the effect of ΔCIE on pCO_2 estimates (for a given ΔpCO_2, lower ΔCIE values yield higher pCO_2 estimates and *vice versa*). $\Delta CIE = -2.5‰$ assumes that *n*-alkanes ($CIE = -5.1‰$; ref. 11) best represent $CIE_{terrestrial}$; $\Delta CIE = -1.6‰$ suggests a smaller offset between $CIE_{terrestrial}$ and CIE_{marine} owing to an underestimation of the magnitude of CIE_{marine} ($CIE_{marine} = -3.1‰$ versus $-2.6‰$). Vertical lines mark ΔpCO_2 estimates for specific proposed sources of the event (green = methane hydrate[14], $\delta^{13}C_{source} = -60‰$; purple = thermogenic methane[54] or permafrost thawing[50], $\delta^{13}C_{source} = -30‰$; and orange = wildfire burning[55] or oxidation of organic matter from drying of epicontinental seas[56], $\delta^{13}C_{source} = -22‰$) based on a mass balance equation (equation (3) and the parameters used by McInerney and Wing[11] (0.3 p.p.m.v. increase in pCO_2 per Pg C added, $\delta^{13}C_{initial} = -2.5‰$, and $M_{initial} = 50{,}000$ Pg C); horizontal arrows mark the range of ΔpCO_2 estimates calculated for each source (equation (3)), provided a range of estimates for the pCO_2 increase per Pg C added (0.23 to 0.39) and estimates of $\delta^{13}C_{initial}$ (-2.5 to $-0.1‰$) (Methods). The range of average Late Palaeocene (60–55Ma) pCO_2 estimates from other proxies (blue bars) are indicated; a single pCO_2 estimate from stomata provides a lower bound on pCO_2 during the PETM (red point and arrow) (references are provided in the Supplementary Information). Dashed lines mark pre-industrial (280 p.p.m.v.) and present-day (393 p.p.m.v.) pCO_2 levels, as well as a model-based projection of pCO_2 in the year 2300 if fossil fuel burning continues unabated (1,900 p.p.m.v.) (ref. 46). Grey-shaded region represents the range of pCO_2 projections for the year 2100 from the IPCC (566–821 p.p.m.v.) (ref. 60).

Based on the fundamental observation of increased carbon isotope fractionation in C_3 land plants in response to elevated pCO_2 levels (Fig. 1), we propose that the larger amplitude CIE recorded in terrestrial substrates results from the primary phenomenon of rising pCO_2 levels. We attribute deviations from the average size of the CIE measured on the same substrate at different sites to local or regional changes in water availability[6,8,18,36], plant composition[16,17,38,52], dissolution[43] and salinity[42]. For these reasons, the average of many CIEs measured across the planet should be used to determine the average magnitude of the marine and terrestrial signals for the purpose of reconciling the magnitude of the event and reconstructing pCO_2 levels.

We further note systematic differences in the magnitude of the CIE within the marine and terrestrial substrates as compiled by McInerney and Wing[11] in their Table 1. Within the marine record, foraminifera (benthic and planktonic) and bulk marine carbonate record the smallest CIE (-2.5 to $-2.7‰$), while algal lipids and bulk marine organic matter record a greater CIE (-3.5 to $-4.1‰$). In terrestrial systems, the smallest CIE is measured in bulk soil organic matter ($-3.5‰$), followed by tooth enamel and plant lipids (-4.8 to $-5.1‰$), with the largest CIE measured in soil carbonate ($-5.5‰$). The greater CIE measured in algal lipids compared with foraminifera is likely caused by elevated pCO_2 levels, as photosynthetic algae are also known to show increasing carbon isotope fractionation with increasing concentrations of CO_2 dissolved in water although these relationships vary widely (reviewed within ref. 53) and differ from that of higher land plants. Bulk organic matter in terrestrial and marine environments show the same median magnitude CIE ($-3.5‰$); the CIE measured in terrestrial bulk organic matter may be dampened relative to other terrestrial substrates by mixing of organic matter of a different age[15], while the marine bulk organic matter CIE is likely augmented compared with other marine substrates by photosynthetic inputs from terrestrial and marine environments[15,28–30]. Variability in the degree of these inputs may explain why bulk marine organic matter shows the greatest variability among all substrates ($1\sigma = \pm 2.2‰$). Within purely terrestrial systems, the median CIE recorded in plant lipids ($-5.0‰$) reflects the full effects of elevated pCO_2 levels on plant isotope fractionation (as shown here and in ref. 26); the similar median CIE recorded in fossil tooth enamel ($-4.9‰$) is not surprising considering that it reflects the $\delta^{13}C$ value of the plants the herbivore consumes. The very large CIE measured in paleosol carbonate (average $= -5.5‰$, median $= -6.3‰$) may reflect a combination of the enhanced fractionation by plants under high pCO_2, diffusion of increased pCO_2 levels into the soil and increased productivity. Based on measurements of enamel carbonate, Secord *et al.*[33] attribute 1.5‰ of the CIE measured in soil carbonate to increased rates of carbon turnover, driven by warmer climate.

Our results illustrate the need to account for changes in pCO_2 concentration when interpreting changes in the carbon isotope composition of substrates derived at least in part from C_3 land plants, which dominate the terrestrial carbon record. Although our analysis was applied specifically to the PETM, the fundamental pCO_2 effect and equations presented here can be applied similarly to other global CIE events recorded in marine and terrestrial sediments (for example, Aptian–Albian, Early Toarcian, Triassic–Jurassic, Permian–Triassic and many others) in order to quantitatively reconstruct levels of pCO_2 before and during the CIE event.

Methods

Quantifying ΔpCO_2. We used the following mass balance equation modified from McInerney and Wing[11] to quantify ΔpCO_2 for each of the proposed sources (vertical, coloured lines in Fig. 3: green = methane hydrate[14], $\delta^{13}C_{source} = -60‰$; purple = thermogenic methane[54] or permafrost thawing[50], $\delta^{13}C_{source} = -30‰$;

and orange = wildfire burning[55] or oxidation of organic matter from drying of epicontinental seas[56], $\delta^{13}C_{source} = -22‰$):

$$\Delta pCO_2 = \frac{-(CIE_{marine})(M_{initial})(0.3)}{\delta^{13}C_{final} - \delta^{13}C_{source}} \quad (3)$$

where M_{inital} is the mass of the Palaeocene surface reservoir, $\delta^{13}C_{final}$ is the $\delta^{13}C$ value at the PETM ($\delta^{13}C_{final} = \delta^{13}C_{initial} + CIE_{marine}$), $\delta^{13}C_{initial}$ is the $\delta^{13}C$ value of the Late Palaeocene carbon pool and $\delta^{13}C_{source}$ is the $\delta^{13}C$ value of the source responsible for the CIE. We used CIE_{marine} (and not $CIE_{terrestrial}$) because it does not incorporate any land-plant-derived components and thus only represents changes in $\delta^{13}C_{CO2}$. The constant 0.3 indicates that for every 1 Pg C added pCO_2 increases 0.3 p.p.m.v. (ref. 11); this value is within the range of values suggested from models of the carbon release at the PETM (for example, 0.23–0.39; refs 12,27,57). We calculated the value for CIE_{marine} ($-2.6‰$) as the average of the CIEs measured in benthic forams ($-2.5 \pm 1.0‰$, $n = 36$), planktic forams ($-2.7 \pm 1.0‰$, $n = 36$) and bulk marine carbonate ($-2.7 \pm 1.1‰$, $n = 33$) as listed in Table 1 of McInerney and Wing[11]. Bulk marine organic matter (CIE = $-4.1 \pm 2.2‰$, $n = 11$) was not included in the average because it may contain a mix of marine and terrestrial inputs[28–30]; the single CIE measured on algal lipids (CIE = $-3.5‰$) was also excluded. Our values for $M_{initial} = 50{,}000$ Pg C and $\delta^{13}C_{initial} = -2.5‰$ were based on the values used by McInerney and Wing[11]. We note, however, that the value for $\delta^{13}C_{initial} = -2.5‰$ may be too low; we estimate $\delta^{13}C_{initial}$ as high as $-0.1‰$ assuming a pre-industrial value of -2.1 to $-2.6‰$ (ref. 14) offset by $+2.0‰$ based on the secular change in $\delta^{13}C$ (ref. 58).

References

1. Hesselbo, S. P., Robinson, S. A., Surlyk, F. & Piasecki, S. Terrestrial and marine extinction at the Triassic-Jurassic boundary synchronized with major carbon-cycle perturbation: a link to initiation of massive volcanism? *Geology* **30,** 251–254 (2002).
2. Koch, P. L., Zachos, J. C. & Gingerich, P. D. Correlation between isotope records in marine and continental carbon reservoirs near the Palaeocene/Eocene boundary. *Nature* **358,** 319–322 (1992).
3. Hesselbo, S. P. *et al.* Carbon-cycle perturbation in the Middle Jurassic and accompanying changes in the terrestrial paleoenvironment. *J. Geol.* **111,** 259–276 (2003).
4. Herrle, J. O., Kößler, P., Friedrich, O., Erlenkeuser, H. & Hemleben, C. High-resolution carbon isotope records of the Aptian to Lower Albian from SE France and the Mazagan Plateau (DSDP Site 545): a stratigraphic tool for paleoceanographic and paleobiologic reconstruction. *Earth Planet Sci. Lett.* **218,** 149–161 (2004).
5. Ruhl, M., Bonis, N. R., Reichart, G.-J., Damsté, J. S. S. & Kürschner, W. M. Atmospheric carbon injection linked to end-Triassic mass extinction. *Science* **333,** 430–434 (2011).
6. Bowen, G. J., Beerling, D. J., Koch, P. L., Zachos, J. C. & Quattlebaum, T. A humid climate state during the Palaeocene/Eocene thermal maximum. *Nature* **432,** 495–499 (2004).
7. Hesselbo, S. P., Jenkyns, H. C., Duarte, L. V. & Oliveira, L. C. V. Carbon-isotope record of the Early Jurassic (Toarcian) Oceanic Anoxic Event from fossil wood and marine carbonate (Lusitanian Basin, Portugal). *Earth Planet Sci. Lett.* **253,** 455–470 (2007).
8. Abels, H. A. *et al.* Terrestrial carbon isotope excursions and biotic change during Palaeogene hyperthermals. *Nat. Geosci.* **5,** 326–329 (2012).
9. Jahren, A. H., Conrad, C. P., Arens, N. C., Mora, G. & Lithgow-Bertelloni, C. A plate tectonic mechanism for methane hydrate release along subduction zones. *Earth Planet Sci. Lett.* **236,** 691–704 (2005).
10. Tipple, B. J. *et al.* Coupled high-resolution marine and terrestrial records of carbon and hydrologic cycles variations during the Paleocene-Eocene Thermal Maximum (PETM). *Earth Planet Sci. Lett.* **311,** 82–92 (2011).
11. McInerney, F. A. & Wing, S. L. The Paleocene-Eocene thermal maximum: a perturbation of carbon cycle, climate, and biosphere with implications for the future. *Annu. Rev. Earth Planet Sci.* **39,** 489–516 (2011).
12. Zeebe, R. E., Zachos, J. C. & Dickens, G. R. Carbon dioxide forcing alone insufficient to explain Palaeocene-Eocene Thermal Maximum warming. *Nat. Geosci.* **2,** 576–580 (2009).
13. Pagani, M., Caldeira, K., Archer, D. & Zachos, J. C. An ancient carbon mystery. *Science* **314,** 1556–1557 (2006).
14. Dickens, G. R., O'Neil, J. R., Rea, D. K. & Owen, R. M. Dissociation of oceanic methane hydrate as a cause of the carbon isotope excursion at the end of the Paleocene. *Paleoceanography* **10,** 965–971 (1995).
15. Sluijs, A. & Dickens, G. R. Assessing offsets between the $\delta^{13}C$ of sedimentary components and the global exogenic carbon pool across early Paleogene carbon cycle perturbations. *Global Biogeochem. Cycles* **26** 10.1029/2011GB004224 doi:10.1029/2011gb004224 (2012).
16. Schouten, S. *et al.* The Paleocene-Eocene carbon isotope excursion in higher plant organic matter: differential fractionation of angiosperms and conifers in the Arctic. *Earth Planet Sci. Lett.* **258,** 581–592 (2007).
17. Smith, F. A., Wing, S. L. & Freeman, K. H. Magnitude of the carbon isotope excursion at the Paleocene-Eocene thermal maximum: the role of plant community change. *Earth Planet Sci. Lett.* **262,** 50–65 (2007).
18. Pagani, M. *et al.* Arctic hydrology during global warming at the Palaeocene/Eocene thermal maximum. *Nature* **442,** 671–675 (2006).
19. Kohn, M. J. Carbon isotope compositions of terrestrial C3 plants as indicators of (paleo)ecology and (paleo)climate. *Proc. Natl Acad. Sci. USA* **107,** 19691–19695 (2010).
20. Edwards, G. E., Furbank, R. T., Hatch, M. D. & Osmond, C. B. What does it take to be C_4? Lessons from the evolution of C_4 photosynthesis. *Plant Physiol.* **125,** 46–49 (2001).
21. Feng, X. & Epstein, S. Carbon isotopes of trees from arid environments and implications for reconstructing atmospheric CO_2 concentration. *Geochim. Cosmochim. Acta* **59,** 2599–2608 (1995).
22. Kürschner, W. M. *Leaf Stomata as Biosensors of Palaeoatmospheric CO_2 Levels.* PhD Thesis, Utrecht University (1996).
23. Wang, W. *et al.* A 200 year temperature record from tree ring $\delta^{13}C$ at the Qaidam Basin of the Tibetan Plateau after identifying the optimum method to correct for changing atmospheric CO_2 and $\delta^{13}C$. *J. Geophys. Res.* **116,** G04022 (2011).
24. Treydte, K. S. *et al.* Impact of climate and CO_2 on a millennium-long tree-ring carbon isotope record. *Geochim. et Cosmochim. Acta* **73,** 4635–4647 (2009).
25. McCarroll, D. *et al.* Correction of tree ring stable isotope chronologies for changes in the carbon dioxide content of the atmosphere. *Geochim. et Cosmochim. Acta* **73,** 1539–1547 (2009).
26. Schubert, B. A. & Jahren, A. H. The effect of atmospheric CO_2 concentration on carbon isotope fractionation in C_3 land plants. *Geochim. et Cosmochim. Acta* **96,** 29–43 (2012).
27. Cui, Y. *et al.* Slow release of fossil carbon during the Palaeocene–Eocene thermal maximum. *Nat. Geosci.* **4,** 481–485 (2011).
28. Schoon, P. L., Sluijs, A., Damsté, J. S. S. & Schouten, S. Stable carbon isotope patterns of marine biomarker lipids in the Arctic Ocean during Eocene Thermal Maximum 2. *Paleoceanography* **26,** PA3215 (2011).
29. Weijers, J. W. H., Schouten, S., Schefuß, E., Schneider, R. R. & Sinninghe Damsté, J. S. Disentangling marine, soil and plant organic carbon contributions to continental margin sediments: a multi-proxy approach in a 20,000 year sediment record from the Congo deep-sea fan. *Geochim. et Cosmochim. Acta* **73,** 119–132 (2009).
30. Gordon, E. S. & Goñi, M. A. Sources and distribution of terrigenous organic matter delivered by the Atchafalaya River to sediments in the northern Gulf of Mexico. *Geochim. et Cosmochim. Acta* **67,** 2359–2375 (2003).
31. Schmitz, B. & Pujalte, V. Abrupt increase in seasonal extreme precipitation at the Paleocene-Eocene boundary. *Geology* **35,** 215–218 (2007).
32. Wing, S. L. *et al.* Transient floral change and rapid global warming at the Paleocene-Eocene boundary. *Science* **310,** 993–996 (2005).
33. Secord, R., Gingerich, P. D., Lohmann, K. C. & MacLeod, K. G. Continental warming preceding the Palaeocene-Eocene thermal maximum. *Nature* **467,** 955–958 (2010).
34. Larrasoaña, J. C. *et al.* Magnetotactic bacterial response to Antarctic dust supply during the Palaeocene–Eocene thermal maximum. *Earth Planet Sci. Lett.* **333–334,** 122–133 (2012).
35. Kraus, M. J. & Riggins, S. Transient drying during the Paleocene-Eocene Thermal Maximum (PETM): analysis of paleosols in the bighorn basin, Wyoming. *Palaeogeogr. Palaeoclimatol. Palaeoecol.* **245,** 444–461 (2007).
36. Handley, L. *et al.* Changes in the hydrological cycle in tropical East Africa during the Paleocene–Eocene Thermal Maximum. *Palaeogeogr. Palaeoclimatol. Palaeoecol.* **329–330,** 10–21 (2012).
37. Storme, J. Y. *et al.* Cycles of humid-dry climate conditions around the P/E boundary: new stable isotope data from terrestrial organic matter in Vasterival section (NW France). *Terr. Nova* **24,** 114–122 (2012).
38. Diefendorf, A. F., Mueller, K. E., Wing, S. L., Koch, P. L. & Freeman, K. H. Global patterns in leaf ^{13}C discrimination and implications for studies of past and future climate. *Proc. Natl Acad. Sci. USA* **107,** 5738–5743 (2010).
39. Winguth, A., Shellito, C., Shields, C. & Winguth, C. Climate response at the Paleocene–Eocene Thermal Maximum to greenhouse gas forcing—A model study with CCSM3. *J. Clim.* **23,** 2562–2584 (2010).
40. John, C. M. *et al.* Clay assemblage and oxygen isotopic constraints on the weathering response to the Paleocene-Eocene thermal maximum, east coast of North America. *Geology* **40,** 591–594 (2012).
41. Foreman, B. Z., Heller, P. L. & Clementz, M. T. Fluvial response to abrupt global warming at the Palaeocene/Eocene boundary. *Nature* **491,** 92–95 (2012).
42. Dickens, G. R. Down the rabbit hole: toward appropriate discussion of methane release from gas hydrate systems during the Paleocene-Eocene thermal maximum and other past hyperthermal events. *Clim. Past* **7,** 831–846 (2011).
43. Zachos, J. C. *et al.* Rapid acidification of the ocean during the Paleocene-Eocene thermal maximum. *Science* **308,** 1611–1615 (2005).

44. McCarren, H., Thomas, E., Hasegawa, T., Röhl, U. & Zachos, J. C. Depth dependency of the Paleocene-Eocene carbon isotope excursion: paired benthic and terrestrial biomarker records (Ocean Drilling Program Leg 208, Walvis Ridge). *Geochem. Geophys. Geosyst.* **9,** Q10008 (2008).
45. Zachos, J. C., Dickens, G. R. & Zeebe, R. E. An early Cenozoic perspective on greenhouse warming and carbon-cycle dynamics. *Nature* **451,** 279–283 (2008).
46. Caldeira, K. & Wickett, M. E. Anthropogenic carbon and ocean pH. *Nature* **425,** 365 (2003).
47. Royer, D. L., Pagani, M. & Beerling, D. J. Geobiological constraints on earth system sensitivity to CO_2 during the Cretaceous and Cenozoic. *Geobiology* **10,** 298–310 (2012).
48. Sluijs, A. *et al.* Environmental precursors to rapid light carbon injection at the Palaeocene/Eocene boundary. *Nature* **450,** 1218–1221 (2007).
49. Lunt, D. J. *et al.* A model for orbital pacing of methane hydrate destabilization during the Palaeogene. *Nat. Geosci.* **4,** 775–778 (2011).
50. DeConto, R. M. *et al.* Past extreme warming events linked to massive carbon release from thawing permafrost. *Nature* **484,** 87–92 (2012).
51. Lourens, L. J. *et al.* Astronomical pacing of late Palaeocene to early Eocene global warming events. *Nature* **435,** 1083–1087 (2005).
52. Diefendorf, A. F., Freeman, K. H., Wing, S. L. & Graham, H. V. Production of n-alkyl lipids in living plants and implications for the geologic past. *Geochim. et Cosmochim. Acta* **75,** 7472–7485 (2011).
53. Royer, D. L., Berner, R. A. & Beerling, D. J. Phanerozoic atmospheric CO_2 change: evaluating geochemical and paleobiological approaches. *Earth Sci. Rev.* **54,** 349–393 (2001).
54. Svensen, H. *et al.* Release of methane from a volcanic basin as a mechanism for initial Eocene global warming. *Nature* **429,** 542–545 (2004).
55. Kurtz, A. C., Kump, L. R., Arthur, M. A., Zachos, J. C. & Paytan, A. Early Cenozoic decoupling of the global carbon and sulfur cycles. *Paleoceanography* **18,** doi:10.1029/2003pa000908 (2003).
56. Higgins, J. A. & Schrag, D. P. Beyond methane: towards a theory for the Paleocene–Eocene Thermal Maximum. *Earth Planet Sci. Lett.* **245,** 523–537 (2006).
57. Panchuk, K., Ridgwell, A. & Kump, L. R. Sedimentary response to Paleocene-Eocene Thermal Maximum carbon release: a model-data comparison. *Geology* **36,** 315–318 (2008).
58. Tipple, B. J., Meyers, S. R. & Pagani, M. Carbon isotope ratio of Cenozoic CO_2: a comparative evaluation of available geochemical proxies. *Paleoceanography* **25,** doi:10.1029/2009pa001851 (2010).
59. Lomax, B. H., Knight, C. A. & Lake, J. A. An experimental evaluation of the use of C_3 $\delta^{13}C$ plant tissue as a proxy for the paleoatmospheric $\delta^{13}CO_2$ signature of air. *Geochem. Geophys. Geosyst.* **13,** Q0AI03 (2012).
60. IPCC. *Climate Change 2001: Synthesis Report*. IPCC, 2001.

Acknowledgements

This work was supported by DOE/BES Grant DE-FG02-09ER16002.

Author contributions

B.A.S. and A.H.J. wrote the paper and analysed the results; B.A.S. developed the equations and methods with advice and assistance from A.H.J.

Additional information

Supplementary Information accompanies this paper at http://www.nature.com/naturecommunications

Competing financial interests: The authors claim no competing financial interests associated with this paper.

Reprints and permission information is available online at http://npg.nature.com/reprintsandpermissions/

How to cite this article: Schubert, B. A. & Jahren, A. H. Reconciliation of marine and terrestrial carbon isotope excursions based on changing atmospheric CO_2 levels. *Nat. Commun.* 4:1653 doi: 10.1038/ncomms2659 (2013).

Supplementary Information

B.A. Schubert and A.H. Jahren. Reconciliation of marine and terrestrial carbon isotope excursions based on changing atmospheric CO_2 levels.

The supplementary information contains two supplementary tables (Supplementary Tables S1 and S2); background for quantifying the relationship between pCO_2 and $\Delta\delta^{13}C_p$; discussion of the previous work to determine the true magnitude of the CIE at the PETM; discussion of the previous proxy estimates of Late Palaeocene and PETM pCO_2 levels; and supplementary references.

Supplementary Table S1 | Carbon isotope data from Lomax et al.[59].			
***p*CO$_2$ (ppmv)**	**$\delta^{13}C_p$ (‰)***	**$\delta^{13}C_{CO2}$ (‰)***	**$\Delta\delta^{13}C_p$ (‰)†**
380	-32.5	-12.0	21.2
760	-43.0	-20.5	23.5
1000	-46.0	-23.0	24.1
1500	-48.5	-24.5	25.2
2000	-52.5	-27.5	26.4
3000	-56.5	-30.5	27.6

*$\delta^{13}C_p$ and $\delta^{13}C_{CO2}$ data were rounded to the nearest 0.5‰ from "high water treatment" (constantly moist compost) experiments presented in Figure 4 within Lomax et al.[59].
†$\Delta\delta^{13}C_p$ calculated according to Equation S2.

Supplementary Table S2 | The amount of fractionation per 100 ppm increase in pCO_2 (S) measured in C_3 land plants.*

S (‰ per 100 ppm)	pCO_2 range (ppm)	Species	Reference
2.70	198 – 243	*Pinus flexilis*	61
2.20	243 – 279	*Pinus flexilis*	61
2.07	303 – 361	*Pinus sylvestris*	62
2.00	300 – 310	Mixed (11)	63
2.00	277 – 351	Mixed (4)	21
1.88	310 – 350	Mixed (11)	63
1.75	380 – 482	*Pinus contortus*	64
1.60	280 – 380	*Sabina przewalskii*	23
1.45	285 – 354	*Swietenia macrophylla*	65
1.20	285 – 365	*Juniperus* spp.	24
1.00	343 – 569	*Quercus ilex*	66
0.96	407 – 497	*Raphanus sativus*	26
0.80	380 – 760	*Arabidopsis thaliana*	59
0.76	370 – 455	*Arabidopsis thaliana*	26
0.73	350 – 700	*Quercus petrea*	22
0.72	497 – 576	*Raphanus sativus*	26
0.62	380 – 607	*Linaria dalmatica*	64
0.48	576 – 780	*Raphanus sativus*	26
0.41	455 – 733	*Arabidopsis thaliana*	26
0.38	760 – 1000	*Arabidopsis thaliana*	59
0.37	350 – 700	Mixed (17)	67
0.21	1000 – 1500	*Arabidopsis thaliana*	59
0.20	733 – 995	*Arabidopsis thaliana*	26
0.20	780 – 1494	*Raphanus sativus*	26
0.12	995 – 1302	*Arabidopsis thaliana*	26
0.11	1500 – 2000	*Arabidopsis thaliana*	59
0.096	1494 – 1766	*Raphanus sativus*	26
0.066	1302 – 1843	*Arabidopsis thaliana*	26
0.060	2000 – 3000	*Arabidopsis thaliana*	59
0.054	1766 – 2723	*Raphanus sativus*	26
0.039	1843 – 2255	*Arabidopsis thaliana*	26
0.029	2723 – 3429	*Raphanus sativus*	26
0.019	3429 – 4200	*Raphanus sativus*	26

*Modified from ref. 26.

Supplementary Methods

Quantifying the relationship between pCO_2 and $\Delta\delta^{13}C_p$

Within C_3 plants (i.e., plants that employ only the RuBisCO enzyme to catalyze CO_2 fixation), the net isotopic difference between the atmospheric CO_2 and the resultant plant tissue has been modeled according to the following equation[68]:

$$\Delta\delta^{13}C_p = a + (b - a)\,(c_i/c_a) \quad \text{(S1)}$$

where

$$\Delta\delta^{13}C_p = (\delta^{13}C_{CO2} - \delta^{13}C_p) / (1 + \delta^{13}C/1000) \quad \text{(S2).}$$

Within the above, the constants a and b represent the isotopic fractionation due to diffusion through the plant's stomata (a = 4.4‰) and subsequent catalysis by RuBisCO (b = 26-30‰), respectively; $\delta^{13}C_p$ and $\delta^{13}C_{CO2}$ are the carbon isotope composition of plant tissue and CO_2 in the atmosphere, respectively; and c_i and c_a are the intracellular and atmospheric concentration of CO_2 (c_a is equivalent to pCO_2), respectively.

Many records of $\Delta\delta^{13}C_p$ in C_3 plant tissues show or imply a positive, linear relationship between $\Delta\delta^{13}C_p$ and pCO_2 for small (10 to 350 ppmv) changes in pCO_2 (e.g., 300 to 310 ppmv or 350 to 700 ppmv) (refs [21-25,61-67,69-72]). The reported slope of this relationship (S) varies widely, with the most cited estimates ranging from S = 0.0073 to 0.020‰/ppmv (S = 0.7 to 2.0‰ per 100 ppmv CO_2). However, extrapolation of these factors to very high pCO_2 levels relevant to the geologic record results in values of carbon isotopic discrimination not seen in the current or fossil record of plant life nor are theoretically possible[26]. Thus, the relationship between $\Delta\delta^{13}C_p$ and pCO_2 cannot continue to increase without plateau, although this has only recently been hinted at in the literature (e.g., ref. 24).

Across a wide range of C_3 species, we found that the increase in $\Delta\delta^{13}C_p$ per unit increase in pCO_2 (slope, S) systematically decreases with increasing pCO_2 according to the following equation (R = 0.95; n = 28) (ref. 26):

$$S = \frac{(A^2)(B)}{[A+(B)(pCO_2+C)]^2} \quad \text{(S3)}$$

where A = 28.26, B = 0.21, and C = 25. This equation indicates that S is not a constant value, as previously reported, but instead approaches zero as the atmosphere becomes saturated with CO_2. Equation (S3) indicates that at pre-industrial levels of pCO_2 (280 ppmv), the response to rising pCO_2 is 0.020‰/ppmv (the same value reported by Feng and Epstein[21] for several tree species growing at 277-351 ppmv), whereas at 560 ppmv, the response is 0.0073‰/ppmv (the same value reported by Kürschner[22] for oak trees growing at 350-700 ppm).

Equation (S3) follows the form of the derivative of a general hyperbolic relationship such that the integral of equation (S3) is a hyperbola with the following equation (Fig. 1 inset):

$$\Delta\delta^{13}C_p = \frac{(A)(B)(pCO_2+C)}{A+(B)(pCO_2+C)} \quad \text{(S4)}$$

The best-fit curve represented by equation (S3) was determined iteratively such that equation (S4) results in $\Delta\delta^{13}C_p$ = 4.4‰ at pCO_2 = 0 ppmv [a within equation (S1)] and $\Delta\delta^{13}C_p$ = 28.26‰ at $pCO_2 = 10^6$ ppmv [(b within equation (S1)] (after Eqn. 4 within ref. 26). The value 28.26‰ therefore represents the asymptote (A), which is based on experiments on *Raphanus sativus* and *Arabidopsis thaliana* grown under controlled conditions at pCO_2 levels up to 4200 ppmv (ref. 26).

Lomax et al.[59] recently published carbon isotope data on *Arabidopsis* grown under six different levels of pCO_2 ranging from 380-3000 ppmv (Supplementary Table S1). Their data show an increase in $\Delta\delta^{13}C_p$ with increasing pCO_2 that closely fits (i.e., R = 0.97) a hyperbolic relationship (*after* Equation S4, with $\Delta\delta^{13}C_p$ = 4.4‰ at pCO_2 = 0 ppmv) where A = 28.18, B = 0.19, and C = 27 [this relationship is nearly identical to the one presented in Equation 6 within Schubert and Jahren[26] and presented here in Figure 1 (inset)]. The fitted equation of the Lomax et al.[59] data was then used to calculate S-values for between each of the pCO_2 levels they used (*after* Schubert and Jahren[26]); the new S-values from the data of Lomax et al.[59] have been added to Figure 1 and are reported in Supplementary Table S2. The addition of these new data did not change the values for A, B, and C reported within Schubert and Jahren[26], and improved the correlation coefficient slightly (R = 0.96; n = 33) (Fig. 1).

Supplementary Discussion

Previous work to determine the true magnitude of the CIE at the PETM

To calculate the amount of carbon added to the atmosphere at the PETM and thus, improve our understanding of feedbacks in the climate system, requires that the "true" magnitude of the CIE is well constrained[13,14]; however whether marine or terrestrial substrates record the true magnitude of the CIE remains highly debated[6,16-18,38,44,52]. Reasons that the terrestrial record might be more reflective of the scale of the event include evidence for dissolution of marine carbonates due to ocean acidification[43] and alteration of foraminifera by dissolution and changes in pH (ref. 18) that would both serve to truncate the CIE when measured in these substrates. However, the average CIEs

measured in planktonic and benthic foraminifera are indistinguishable (-2.7 ± 1.0‰ vs. -2.5 ± 1.0‰; ref. 11) despite the surface ocean pH being more responsive to increases in CO_2 (due to the already high CO_2 levels present in the deep ocean). We note, however, that the magnitude of the CIE measured in thermocline-dwelling planktonic foraminifera was not distinguished from other planktonic foraminifera in the review by McInerney and Wing[11]. Although examples of large, negative CIEs in marine records do exist (e.g., refs [48,73]), increased runoff and decreased salinity during the PETM may have led to these anomalously large excursion values (see ref. 42).

Other researchers have concluded that the larger CIE measured in terrestrial substrates reflects additional carbon isotope fractionation in land plants that resulted from ancillary changes in global humidity[6], plant communities[16,17], or both[38], and therefore substrates derived from land plants overestimate the true magnitude of the CIE. However, the response of the hydrological cycle at the PETM varied worldwide, with some sites showing drying trends or cycles of changing relative humidity[34-37] and others showing no evidence for any changes at all[74]. Likewise, synchronous shifts in plant communities had to have occurred globally because terrestrial CIEs of the same magnitude have been measured elsewhere[18], and large terrestrial CIEs have been measured at tropical sites where no evidence for significant gymnosperm communities exists prior to the PETM[75]. Even if gymnosperms did dominate a site in the Late Paleocene, their input to the *n*-alkane record is significantly smaller than angiosperm plants and therefore cannot account for the increased CIE observed on land[52]. McCarren et al.[44] suggested that the true CIE lies somewhere between the 3.5‰ magnitude they recorded in benthic

foraminifera and the 5‰ excursion measured in *n*-alkanes from the same site; Sluijs and Dickens[15] suggest that the CIE was likely <4‰.

In order to account for a larger CIE that has been measured within terrestrial substrates and the significant temperature increase at the PETM, several sources, beyond the original methane release hypothesis of Dickens et al.[14], have been proposed[13] [e.g., comet[76], thermogenic methane[54], thawed permafrost[50], wildfires[55], and oxidation of organic matter from drying epicontinental seas[56]]. These alternative hypotheses generally assume that terrestrial substrates more closely record the true magnitude of the CIE, although calculations for the amount of carbon released assuming each of these proposed sources remain valid for a smaller CIE as measured in marine substrates.

Previous proxy estimates of Late Palaeocene and PETM pCO_2 levels

Previous proxy estimates for Late Palaeocene pCO_2 cover a wide range of values (100-2400 ppmv) (Fig. 3). A previous, poorly-constrained estimate of pCO_2 levels at the PETM based on stomatal indices indicated pCO_2 ≥800 ppmv[77] and early work by Koch et al.[2] did not identify an increase in pCO_2 levels at the CIE above background levels (≤350 ppmv). pCO_2 data from liverwort, phytoplankton, and stomatal proxies were compiled from refs [78,79]; pCO_2 data determined using the boron isotope proxy are from ref. [80]. Late Palaeocene pCO_2 estimates from paleosols represent the data reported in ref. [81] and include pCO_2 estimates below pre-industrial levels.

Supplementary References

61 Van de Water, P. K., Leavitt, S. W. & Betancourt, J. L. Trends in stomatal density and $^{13}C/^{12}C$ ratios of *Pinus flexilis* needles during last glacial-interglacial cycle. *Science* **264**, 239-243 (1994).

62 Berninger, F., Sonninen, E., Aalto, T. & Lloyd, J. Modeling ^{13}C discrimination in tree rings. *Global Biogeochemical Cycles* **14**, 213-223 (2000).

63 Peñuelas, J. & Estiarte, M. Trends in plant carbon concentration and plant demand for N throughout this century. *Oecologia* **109**, 69-73 (1997).

64 Sharma, S. & Williams, D. G. Carbon and oxygen isotope analysis of leaf biomass reveals contrasting photosynthetic responses to elevated CO_2 near geologic vents in Yellowstone National Park. *Biogeosciences* **6**, 25-31 (2009).

65 Hietz, P., Wanek, W. & Dünisch, O. Long-term trends in cellulose $\delta^{13}C$ and water-use efficiency of tropical *Cedrela a*nd *Swietenia* from Brazil. *Tree Physiol.* **25**, 745-752 (2005).

66 Saurer, M., Cherubini, P., Bonani, G. & Siegwolf, R. Tracing carbon uptake from a natural CO_2 spring into tree rings: an isotope approach. *Tree Physiol.* **23**, 997-1004 (2003).

67 Beerling, D. J. & Woodward, F. I. Leaf stable carbon isotope composition records increased water-use efficiency of C_3 plants in response to atmospheric CO_2 enrichment. *Functional Ecology* **9**, 394-401 (1995).

68 Farquhar, G. D., Ehleringer, J. R. & Hubick, K. T. Carbon isotope discrimination and photosynthesis. *Annual Rev. of Plant Physiol. and Plant Molecular Biol.* **40**, 503-537 (1989).

69 Kirdyanov, A. V., Treydte, K. S., Nikolaev, A., Helle, G. & Schleser, G. H. Climate signals in tree-ring width, density and $\delta^{13}C$ from larches in Eastern Siberia (Russia). *Chemical Geology* **252**, 31-41, doi:10.1016/j.chemgeo.2008.01.023 (2008).

70 Loader, N. J. *et al.* Multiple stable isotopes from oak trees in southwestern Scotland and the potential for stable isotope dendroclimatology in maritime climatic regions. *Chemical Geology* **252**, 62-71, doi:10.1016/j.chemgeo.2008.01.006 (2008).

71 Gagen, M. *et al.* Exorcising the 'segment length curse': Summer temperature reconstruction since AD 1640 using non-detrended stable carbon isotope ratios from pine trees in northern Finland. *Holocene* **17**, 435-446, doi:10.1177/0959683607077012 (2007).

72 Beerling, D. J., Mattey, D. P. & Chaloner, W. G. Shifts in the $\delta^{13}C$ composition of *Salix herbacea* L. leaves in response to spatial and temporal gradients of atmospheric CO_2 concentration. *Proc. R. Soc. London, Ser. B* **253**, 53-60 (1993).

73 Zachos, J. C. *et al.* Extreme warming of mid-latitude coastal ocean during the Paleocene-Eocene Thermal Maximum: Inferences from TEX_{86} and isotope data. *Geology* **34**, 737-740, doi:10.1130/g22522.1 (2006).

74 Jaramillo, C. *et al.* Effects of rapid global warming at the Paleocene-Eocene boundary on neotropical vegetation. *Science* **330**, 957-961, doi:10.1126/science.1193833 (2010).

75 Handley, L., Pearson, P. N., McMillan, I. K. & Pancost, R. D. Large terrestrial and marine carbon and hydrogen isotope excursions in a new Paleocene/Eocene

boundary section from Tanzania. *Earth and Planetary Science Letters* **275**, 17-25, doi:10.1016/j.epsl.2008.07.030 (2008).

76 Kent, D. V. *et al.* A case for a comet impact trigger for the Paleocene/Eocene thermal maximum and carbon isotope excursion. *Earth and Planetary Science Letters* **211**, 13-26, doi:10.1016/s0012-821x(03)00188-2 (2003).

77 Royer, D. L. *et al.* Paleobotanical evidence for near present-day levels of atmospheric CO_2 during part of the Tertiary. *Science* **292**, 2310-2313, doi:10.1126/science.292.5525.2310 (2001).

78 Royer, D. L. CO_2-forced climate thresholds during the Phanerozoic. *Geochim. et Cosmochim. Acta* **70**, 5665-5675 (2006).

79 Royer, D. L., Pagani, M. & Beerling, D. J. Geobiological constraints on Earth system sensitivity to CO_2 during the Cretaceous and Cenozoic. *Geobiology* **10**, 298-310, doi:10.1111/j.1472-4669.2012.00320.x (2012).

80 Demicco, R. V., Lowenstein, T. K. & Hardie, L. A. Atmospheric pCO_2 since 60 Ma from records of seawater pH, calcium, and primary carbonate mineralogy. *Geology* **31**, 793-796 (2003).

81 Breecker, D. O., Sharp, Z. D. & McFadden, L. D. Atmospheric CO_2 concentration during ancient greenhouse climates were similar to those predicted for A.D. 2100. *Proceedings of the National Academy of Sciences USA* **107**, 576-580 (2010).